Contribution of tropical cyclones to the air-sea CO2 flux: A global view

Marina Lévy, Matthieu Lengaigne, Laurent Bopp, Emmanuel M. Vincent, Gurvan Madec, Christian Éthé, D. Kumar, V. V. S. S. Sarma

Contribution of tropical cyclones to the air-sea CO_2 flux: A global view

M. Lévy,[1] M. Lengaigne,[1,2] L. Bopp,[3] E. M. Vincent,[1] G. Madec,[1,4] C. Ethé,[5] D. Kumar,[2] and V. V. S. S. Sarma[6]

Received 16 June 2011; revised 16 December 2011; accepted 27 January 2012; published 7 April 2012.

[1] Previous case studies have illustrated the strong local influence of tropical cyclones (TCs) on CO_2 air-sea flux (F_{CO_2}), suggesting that they can significantly contribute to the global F_{CO_2}. In this study, we use a state-of-the art global ocean biochemical model driven by TCs wind forcing derived from a historical TCs database, allowing to sample the F_{CO_2} response under 1663 TCs. Our results evidence a very weak contribution of TCs to global F_{CO_2}, one or two order of magnitude smaller than previous estimates extrapolated from case studies. This result arises from several competing effects involved in the F_{CO_2} response to TCs, not accounted for in previous studies. While previous estimates have hypothesized the ocean to be systematically oversaturated in CO_2 under TCs, our results reveal that a similar proportion of TCs occur over oversaturated regions (i.e. the North Atlantic, Northeast Pacific and the Arabian Sea) and undersaturated regions (i.e. Westernmost North Pacific, South Indian and Pacific Ocean). Consequently, by increasing the gas exchange coefficient, TCs can generate either instantaneous CO_2 flux directed from the ocean to the atmosphere (efflux) or the opposite (influx), depending on the CO_2 conditions at the time of the TC passage. A large portion of TCs also occurs over regions where the ocean and the atmosphere are in near equilibrium, resulting in very weak instantaneous fluxes. Previous estimates also did not account for any asynchronous effect of TCs on F_{CO_2}: during several weeks after the storm, oceanic pCO_2 is reduced in response to vertical mixing, which systematically causes an influx anomaly. This implies that, contrary to previous estimates, TCs weakly affect the CO_2 efflux when they blow over supersaturated areas because the instantaneous storm *wind effect* and post-storm *mixing effect* oppose with each other. In contrast, TCs increase the CO_2 influx in undersaturated conditions because the two effects add up. These compensating effects result in a very weak contribution to global F_{CO_2} and a very modest contribution to regional interannual variations (up to 10%).

Citation: Lévy, M., M. Lengaigne, L. Bopp, E. M. Vincent, G. Madec, C. Ethé, D. Kumar, and V. V. S. S. Sarma (2012), Contribution of tropical cyclones to the air-sea CO_2 flux: A global view, *Global Biogeochem. Cycles*, *26*, GB2001, doi:10.1029/2011GB004145.

1. Introduction

[2] Tropical cyclones (TCs), also often called typhoons in the Northwest Pacific or hurricanes on the eastern side of the dateline, are recurring extreme summertime weather events which strongly affect the thermal and physical structure of the upper ocean along their wake [e.g., *D'Asaro*, 2003; *Cione and Uhlhorn*, 2003]. One of the strong oceanic response commonly observed in the wake of TCs is the intense cooling of the surface layer that can reach up to 10°C [*Chiang et al.*, 2011]. This cooling mainly ensues from the wind-driven vertical entrainment of cold subsurface waters [*Price*, 1981; *Vincent et al.*, 2012].

[3] A few previous case studies have illustrated that TCs can cause enormous effluxes of CO_2 between the ocean and atmosphere (hereafter F_{CO_2}), large enough to influence the annual local efflux [*Bates et al.*, 1998; *Perrie*, 2004; *Nemoto et al.*, 2009]. Although TCs are short-lived and travel at considerable speed (typically 4–6 m/s), they affect a significant area of the tropical ocean each year, because of their large spatial extent (several ~100 km) [*Willoughby et al.*, 2006] and frequent occurrence (~100 TCs each year). It was thus hypothesized that they exert a significant influence on the global air-sea flux of CO_2 [*Bates et al.*, 1998]. However, the limited availability of pCO_2 data under TCs

[1]LOCEAN-IPSL, CNRS/IRD/UPMC/MNHN, Paris, France.
[2]National Institute of Oceanography, Goa, India.
[3]LSCE-IPSL, CNRS/CEA/UVSQ, Gif-sur-Yvette, France.
[4]NOCS, Southampton, UK.
[5]IPSL, CNRS/IRD/UPMC/UVSQ/CEA/Ecole Polytechnique/ENS/CNES/UDD/UPEC, Guyancourt, France.
[6]National Institute of Oceanography, Visakhapatnam, India.

0886-6236/12/2011GB004145

(due to the severe weather conditions) has so far restricted the global quantification of the F_{CO_2} response to TCs to qualitative extrapolations [*Bates et al.*, 1998; *Bates*, 2007; *Huang and Imberger*, 2010].

[4] The F_{CO_2} response to a hurricane passage depends on various factors. F_{CO_2} is a function of piston velocity and of the difference in the partial pressure of CO_2 (pCO_2) between the atmosphere and sea surface. Oceanic pCO_2 depends on total dissolved inorganic carbon (DIC), total alkalinity (TA), temperature (T) and salinity (S) [*Takahashi et al.*, 1993]. TCs increase the magnitude of the F_{CO_2} because the piston velocity strongly increases at high wind speed [*Liss and Merlivat*, 1986; *Wanninkhof*, 1992; *D'Asaro and McNeil*, 2007; *McNeil and D'Asaro*, 2007]. TCs also impact F_{CO_2} because their intense surface winds increase vertical entrainment of subsurface waters (hereafter referred to as mixing) and thereby change the surface properties of T, S, DIC and TA and thus surface oceanic pCO_2. In addition, the net F_{CO_2} response to TCs is complicated by the fact that the TC-induced mixing (affecting the pCO_2) and TC-winds (affecting the piston velocity) are not synchronous [*Nemoto et al.*, 2009]: cooling, the manifestation of vertical mixing, is observed to be maximum between one and three days after the TC-passage [*Vincent et al.*, 2012] because it largely results from shear mixing driven by near-inertial currents which persist for a few days in the wake of TCs, and its intensity depends on the local vertical structure of the upper ocean (E. M. Vincent et al., Assessing the oceanic control on the amplitude of sea surface cooling induced by tropical cyclones, submitted to *Journal of Geophysical Research*, 2011).

[5] These considerations highlight the difficulty in generalizing the F_{CO_2} response to TCs from individual cases and illustrate why the few global TC-induced F_{CO_2} estimates [*Bates et al.*, 1998; *Bates*, 2007; *Huang and Imberger*, 2010] are so disparate: from ~0.5 PgC to ~0.05 PgC per year. This paper proposes an original methodology and a model framework for accurately quantifying the TC-induced F_{CO_2} and the various processes into play. We use a global Ocean General Circulation Model (NEMO) [*Madec*, 2008] coupled with a biogeochemical model (PISCES) [*Aumont and Bopp*, 2006] with a modified version of CORE forcing [*Large and Yeager*, 2009] that includes an analytic formulation of 2-dimensional TC winds along observed TC tracks [*Vincent et al.*, 2012]. We compare two model simulations, with and without TCs, and provide quantitative diagnostics averaged along the tracks of TCs. This enables us to provide a global picture of the effects of hurricanes on air-sea CO_2 transfers.

2. Model and Methods

2.1. Coupled Hydrodynamic and Carbon Model

[6] The hydrodynamical model used here is the global configuration (ORCA2) of Nucleus for European Modelling of the Ocean (NEMO, v3.2) [*Madec*, 2008]. The quasi-isotropic grid has a nominal resolution of 2° with increased 0.5° latitudinal resolution at the equator. In the vertical, 31 levels are used, with 10 levels in the upper 100 m. The mixed layer dynamics is parameterized using an improved Turbulent Kinetic Energy (TKE) closure scheme with a Langmuir cell, a surface wave breaking parameterization and an energetically consistent time and space discretization [*Madec*, 2008]. Additional subgrid-scale mixing parameterizations include a Laplacian viscosity, an isoneutral Laplacian diffusivity and the use of a GM-scheme to mimic the effect of subgrid-scale eddy processes [*Gent and McWilliams*, 1990]. Complete description of ORCA2 can be found in *Cravatte et al.* [2007].

[7] The Pelagic Interaction Scheme for Carbon and Ecosystem Studies (PISCES, *Aumont and Bopp*, 2006) is coupled to ORCA2. PISCES includes a simple representation of the marine ecosystem and describes the cycles of carbon and of the main marine nutrients (N, P, Fe and Si). The model has 24 compartments. Four living pools are represented: two phytoplankton size classes/ groups (nanophytoplankton and diatoms) and two zooplankton size classes (microzooplankton and mesozooplankton). Fixed Redfield ratios are employed for N and P, while the ratios of both Si, and Fe, to C vary dynamically as a function of the phytoplankton functional group and environmental variables. The carbonate chemistry follows the Ocean Carbon-Cycle Model Intercomparison Project (OCEMIP) protocols (http://www.ipsl.jussieu.fr/OCMIP). The air-sea CO_2 exchange is calculated with the bulk exchange formula:

$$F_{CO_2} = k\,s\,DpCO_2 \tag{1}$$

where F_{CO_2} is the air-sea CO_2 flux with positive values indicating CO_2 goes within the ocean, k is the gas transfer velocity, s is the CO_2 solubility and $DpCO_2 = pCO_2^{atm} - pCO_2^{sea}$ is the difference of pCO_2 between the ocean and atmosphere. In the following, we will use the notation pCO_2 for pCO_2^{sea}. There is still large uncertainty in k, particularly under hurricane winds [*McNeil and D'Asaro*, 2007; *D'Asaro and McNeil*, 2007]. Following the discussion by *McNeil and D'Asaro* [2007], we used the relationship of *Wanninkhof* [1992] to calculate k, which provides a lower limit for k under extreme winds compared to other recent formulations [*Perrie*, 2004].

2.2. Model Setup and Experimental Design

[8] The surface boundary conditions used for the present ORCA2-PISCES simulations are based on the version 2 of the atmospheric data sets and formulations developed by *Large and Yeager* [2009] for global ocean-ice models and are referred to as Coordinated Ocean-ice Reference Experiments (CORE) forcing [*Griffies et al.*, 2009]. The forcing data sets are based on a combination of NCEP/NCAR reanalysis products for the years 1958–2007 with various satellite data sets, and involve adjustments that correct global imbalances (e.g., produce near zero global mean heat and freshwater fluxes when used in combination with observed SSTs). Turbulent fluxes are computed from the CORE bulk formulae as a function of the prescribed atmospheric state and the simulated ocean surface state (SST and surface currents). A bound to 33 m s^{-1} has been introduced to the CORE dimensionless surface drag coefficient (C_D) to account for its observed saturation at strong winds following *Donelan* [2004]. Data are prescribed at six-hourly (wind speed, humidity and atmospheric temperature), daily (short- and long-wave radiation) and monthly (rain and snow) resolution, with inter-annual variability over the time range 1958 to 2007 except for runoff which are kept climatological. To avoid an artificial model drift due to a freshwater imbalance, the sea surface salinity is damped towards

monthly-mean climatological values with a piston velocity of 50 m per 300 days [*Griffies et al.*, 2009].

[9] Boundary conditions for the biogeochemical model include atmospheric dust (Fe) deposition, rivers (Fe, N, P, Si and C) and sediment (Fe) mobilization. These sources are described by *Aumont and Bopp* [2006] and kept constant for the duration of the simulation.

[10] Our simulations start in 1978. For the initial state, we used physical and biogeochemical tracers initialized from previous ORCA2-PISCES experiments: the spun-up physical state was obtained by running a 120-year simulation, starting from Levitus and forced by repeating the 50-year CORE forcing; the biogeochemical state was obtained by running a transient 1870–1977 simulation with increasing pCO_2^{atm} levels following historical records.

[11] From 1978 onwards, we performed two simulations: one with the full strength of TCs (Cyclone or C run) and one without TCs (No cyclone or N run). For these simulations, the 10-m wind forcing from CORE has been modified following *Vincent et al.* [2012]: In the N run, the effect of the weaker than observed TC-like vortices seen in the original CORE forcing has been filtered out by applying a 11-day running mean to the wind components within 600 km of each cyclone. In the C run, analytical TCs have been superimposed to the filtered CORE winds. To do so, TC winds are parameterized using the idealized *Willoughby and Rahn* [2004] TC wind spatial pattern, which is based on a statistical fit to the observed TC winds [*Willoughby et al.*, 2006]. Note that the translation speed of the storm is not accounted for in this idealized wind pattern. Although the translation speed is known to affect the wind asymmetry, the study by *Samson et al.* [2009] indeed suggests that it has a limited effect on the cold wake asymmetry and can be neglected. This idealized wind pattern is interpolated in time at each model time step using the position and maximum wind speed of each cyclone in the IBTrACs database (http://www.ncdc.noaa.gov/oa/ibtracks). This analytical formulation enables to correct for the underestimation of the strength of TC-winds in CORE. An illustration of the different wind forcings (CORE, N and C) under a TC is provided by *Vincent et al.* [2012, Figure 1].

[12] Daily model outputs were saved from 1993 onward. Our analysis are thus based on the 1993–2007 period, and sample the ocean's response to 1663 TCs.

2.3. Observational Data Set

[13] We use a blend of Tropical Rainfall Measuring Mission (TRMM) Microwave Imager (TMI) and Advanced Microwave Scanning Radiometer AMSR-E SST daily data set (http://www.ssmi.com/sst) at a 1/4° horizontal resolution to evaluate the modeled SST response under TCs over the 1998–2007 period. Despite its inability to retrieve SST data under heavy precipitation [*Wentz et al.*, 2000], TMI and AMSR-E offer the advantage of being insensitive to atmospheric water vapor and provide accurate observations of SST beneath clouds, a few days before and after TC passage. The inner-core cooling (i.e. cooling under the eye) cannot be assessed confidently with TMI-AMSR; data are most of the time missing in a 400 km radius around the current TC position. This data set however provides a reliable estimate of the cooling in the TCs wake, data being typically available 1 to 2 days after TC passage. It has however to be noted that the cooling amplitude in the TCs' wake may not be fully captured by this data set, especially for slow moving TCs.

[14] For pCO2, we use the unique concomitant, open-ocean SST and pCO2 observations before and after the passage of a TC that were reported at the BATS site in the north Atlantic (31°50′ N, 64°10′ W) by *Bates et al.* [1998].

2.4. Diagnostics of Oceanic Anomalies Generated by TCs Along Their Tracks

[15] The anomalies of a given oceanic variable V (where V is for instance the SST or pCO_2) ensuing from the passage of TCs, noted ΔV, are computed under each TC track. To compute ΔV, the seasonal cycle of V is first removed from V, leading to a seasonally "de-meaned" V. TC track locations, available at 6h intervals, are used to retrieve V at the surface of the ocean. To characterize the amplitude of the ocean response around each TC-track position, we compute $\mathcal{V}$, the average of seasonally "de-meaned" V over a fixed radius of 200 km (about 3–4 radius of maximum wind) around the track position. We do this averaging because the impact of TCs on sea-surface properties is not restricted to a narrow path along the storm's center but rather can occur in a swath hundreds of kilometers wide, as reported for instance by *Bond et al.* [2011]. The reference unperturbed pre-storm conditions ($\mathcal{V}_{before}$) is defined as the average of $\mathcal{V}$ over 10 to 3 days prior to TC passage. The evolution of the ocean response anomaly at time t to a TC is then defined as $\Delta V(t) = \mathcal{V}(t) - \mathcal{V}_{before}$. The post-storm anomalies $\Delta V(t)$ are generally maximum within 1 to 4 days after the TC passage (section 3.1). We define $\mathcal{V}_{after}$ as the mean value of $\mathcal{V}$ over days 1 to 4 after TC passage, and the wake anomaly as $\overline{\Delta V} = \mathcal{V}_{after} - \mathcal{V}_{before}$ (dashed vertical lines in Figure 1).

[16] This methodology is applied to the model runs and to satellite observations of SST. In the N-run, where TCs have been smoothed out, ΔV_N is close to zero but is not strictly equal to zero because of the presence of variability not due to TCs. This background variability is present in both the C and N runs. To remove it from our estimates of ΔV, for model variables we define $\widetilde{\Delta} V$ as $\widetilde{\Delta} V = \Delta V_C - \Delta V_N$, where subscripts N and C refer to the model solutions of the N and C runs, respectively. Removing ΔV_N does not change our main results and reduces the dispersion (not shown).

2.5. Air-Sea Flux Anomaly Diagnostics

[17] Anomalies in F_{CO_2} in response to TCs (ΔF_{CO_2}) can result either from changes in the wind (and thus in gas transfer velocity Δk) or from changes in mixing (and thus in $\Delta(sDpCO_2)$):

$$\Delta F_{CO_2} = \underbrace{\Delta k \times sDpCO_2}_{\text{wind effect}} + \underbrace{k \times \Delta(sDpCO_2)}_{\text{mixing effect}} \qquad (2)$$

[18] Using the results from the C and N runs, the wind and mixing effects are approximated as :

$$\Delta k \times sDpCO_2 \simeq (k_C - k_N) \times s_N (DpCO_2)_N \qquad (3)$$

and

$$k \times \Delta(sDpCO_2) \simeq k_N \times (s_C (DpCO_2)_C - s_N (DpCO_2)_N) \qquad (4)$$

where subscripts N and C refer to the model solutions of the N and C runs, respectively. Note that the second order terms

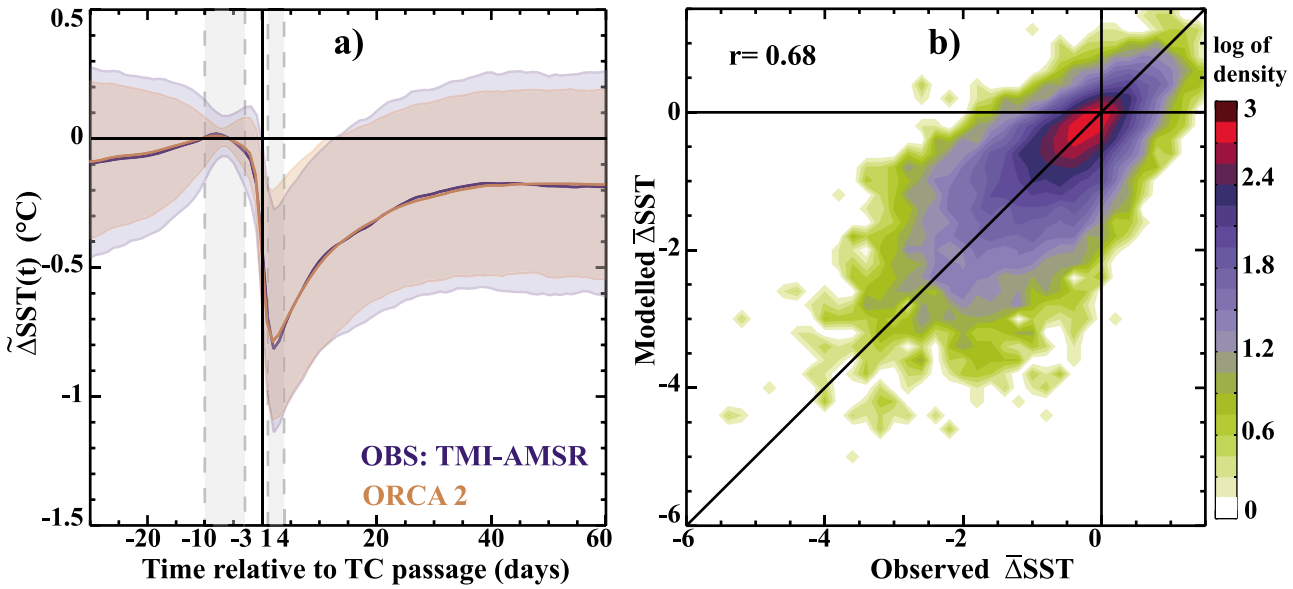

Figure 1. Evaluation of the timing and amplitude of surface temperature response to TCs (a) Temporal evolution of the mean TC-induced cooling along TC tracks for model and observations over the period 1998–2007. Shading indicates the spread around the mean value, calculated as ±1/2 quartile. (b) Scatterplot (shown as a probability density function) of the amplitude of modeled (C-run minus N-run) against observed (TMI-AMSR) TC-induced cold wake amplitude (computed as explained in section 2.4) at individual locations in the wake of TCs.

have been omitted in this approximation; a posteriori, our results show that they are smaller than the first order terms.

3. Model Evaluation

3.1. Evaluation of TC-Induced Cooling

[19] The C run accurately captures the temporal evolution of the average observed TC-induced cooling (Figure 1a). In both model and observation, SST, averaged over a 200 km radius, starts decreasing a few days before the TC reaches a given location (Day 0) and maximum cooling occurs after the TC passage. Although maximum cooling appears to occur 1 to 3 days after the TC passage on Figure 1a for both model and observations, the exact timing of the maximum cooling after the TC passage cannot be confidently validated due to numerous missing satellite SST data around the time of TC passage. However, the fact that maximum cooling is reached a few days after the passage of the storm agrees with previous observations from buoy measurements [*Dickey*, 2008; *Cione and Uhlhorn*, 2003] and models [*Samson et al.*, 2009; *Jullien et al.*, 2012]. The reason is that the cooling largely results from shear mixing driven by near-inertial currents.

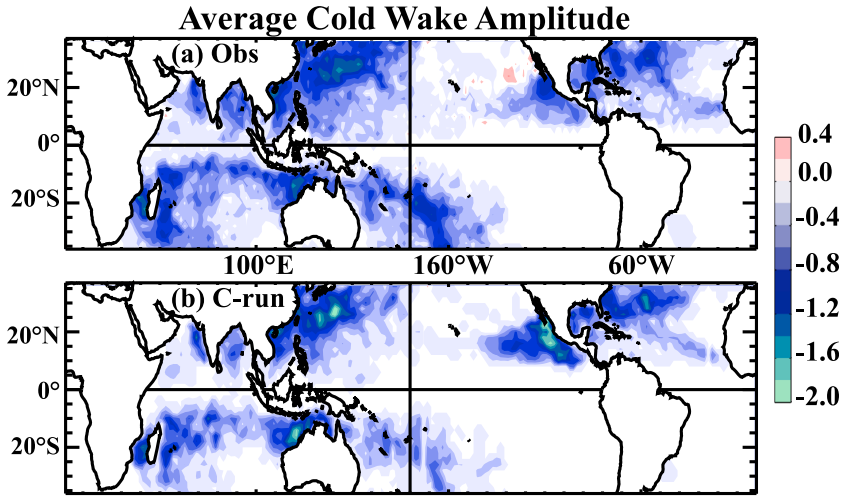

Figure 2. Evaluation of the spatial distribution of the surface temperature response to TCs. Spatial map of averaged cold wake anomaly amplitude (in °C) during the cyclonic season over the 1998–2007 period for (a) TMI-AMSR observations and (b) C-run.

These currents have a period of about a day and last for a few days in the wake of the tropical cyclones so that mixing is still acting to cool the mixed layer a few days after its passage. Figure 1a also illustrates that the decaying time scale of the cooling is accurately simulated, with about 40 days for the SST signal to disappear. The persistence of the cold anomaly for several weeks after the TC passage reflects the time needed for surface heat fluxes to restore the SST to pre-storm values. We can also note that, after 40 days, SST remains on average 0.2°C colder than during pre-storm conditions, in agreement with previous observational analysis [*Price et al.*, 2008; *Lloyd and Vecchi*, 2011; *Vincent et al.*, 2012].

[20] Based on this composite picture, the average value of the e-folding time (time for the cold anomaly to be reduced by a factor e) is 15 days. Moreover, there is a 0.68 correlation between modeled and observed TC-induced cooling magnitudes ($\overline{\Delta}$T) in the wake of TCs at individual locations (Figure 1b), indicating that our simulation realistically samples the ocean response to the wide spectrum of TC characteristics. Because the analytic cyclone wind field formulation is fitted to an average of observed cyclone wind radial profiles [*Willoughby and Rahn*, 2004], and because the underlying ocean state does not exactly match the observed one (biases, missing oceanic eddies), we however do not expect each simulated cold wake to perfectly match the corresponding observed one, as illustrated by the spread on Figure 1b. The model also successfully reproduces the observed spatial distribution of the TC-induced cooling (Figure 2): the average cooling within TC-active regions is about 1°C in all basins, with maximum amplitude of about 2°C in the north-west Pacific region where amongst the most intense TCs occur. The main model deficiency lies in the North-East Pacific basin where modeled coolings are overestimated by almost 1°C. This bias can be tracked back to a shallower than observed thermocline in this region. The use of a coarse horizontal resolution (2°) in our simulation does not hinder the realism of the ocean response to TCs: similar comparisons to observations have indeed been obtained with a simulation of higher (0.5°) resolution using similar boundary conditions and forcing strategy [*Vincent et al.*, 2012, Figure 5].

3.2. Evaluation of the $DpCO_2$

[21] Simulated $DpCO_2$ has been evaluated against observations-based climatologies in *Aumont and Bopp* [2006] both in terms of annual-mean, seasonal amplitude and phasing. Here, we focus on the mean $DpCO_2$ during the TC-season, i.e. from November to April in the southern hemisphere and from May to October in the northern hemisphere (Figure 3). The TC-season $DpCO_2$ displays regions both with positive and negative values qualitatively well reproduced by the model. Regions with negative $DpCO_2$ (oceanic sources of CO_2 to the atmosphere) are in the tropical eastern Pacific, the tropical Atlantic, the Arabian sea. Regions with positive $DpCO_2$ (oceanic sinks for atmospheric CO_2) are found off the west coast of Australia, in the Southwest Pacific and in the mid-latitudes of all oceanic basins.

4. Results

4.1. Case of TC Felix at Station BATS

[22] The observations of *Bates et al.* [1998] at station BATS (31°10′N, 64°10′W) in the Western North Atlantic before and after the passage of TC Felix provide a unique opportunity to evaluate the response in pCO_2 predicted by our model. Around BATS, typical summertime conditions are characterized by weak winds and seawater pCO_2 larger than atmospheric pCO_2^{atm} levels, causing a small flux from ocean to atmosphere. Felix passed over the station on 14–15 August 1995. It was quite large (350 km in diameter) and had sustained winds of 40–45 m s^{-1}. For several weeks before the storm, the SST was close to 28°C and pCO_2 ranged from 400–420 μatm. A sharp decrease of SST and pCO_2 occurred following the TC passage, with similar amplitudes in both model and observations (resp. −3C and −45 μatm). The SST and pCO_2 rebounded after passage of Felix, but did not return to pre-storm values (data from *Bates et al.* [1998], reproduced in Figures 4a and 4b). The oceanic response to Felix is hence successfully captured by our simulation. We should note however that the absolute pCO_2 values display a systematic $\sim$ 10 μatm shift compared to observations (Figure 4b). This shift could be due to the coarse model resolution (2°) used here. This resolution implies that model data represent an average over a 2° region around station BATS, which is characterized by large horizontal gradients of all fields.

[23] The TC passage results in significant changes of the modeled F_{CO_2} (Figure 4c). In the C-run, the F_{CO_2} peaks very abruptly during the 2-days corresponding to the TC passage (August 14–15) reaching 58 mmole/m^2/day, then nearly vanishes (from August 16–29) until three other storms hit the area (in September). In the N-run, the F_{CO_2} do not experience any large variations during the passage of the main TC and of the subsequent storms compared to the C-run, but is larger during the more quiet periods (Figures 4c and 4d).

[24] To interpret the differences of F_{CO_2} between the 2 runs, the wind and mixing effects have been separated according to equations (2), (3), and (4) applied at the fixed location of BATS (Figure 4d). This diagnostics clearly reveals that the wind effect is the driver of the strong increase of F_{CO_2} during the 2 days of the TC-passage and of the three subsequent storms (green curve in Figure 4d). On the other hand, the mixing effect (blue curve in Figure 4c) acts to increase the pCO_2 and thus to reduce the $DpCO_2$, which reduces the F_{CO_2}; moreover, the mixing effect is lagged and lasts longer compared to the wind effect, reducing F_{CO_2} for more than 2 weeks reaching a maximum 2–3 days after the passage of Felix.

[25] The F_{CO_2} caused by Felix has been previously estimated by *Bates et al.* [1998], by assuming that the oceanic pCO_2 was constant in the lead up of the storm, then decreased linearly to the end of the hurricane. This led to a total flux of 40 mmoleC m^{-2} during the two-days passage of the storm; this estimate did not account for the flux reduction during post-hurricane conditions. With our model, we predict a $\tilde{\Delta}F_{CO_2}$ of 62 mmoleC m^{-2} during the storm. This larger number compared with to *Bates et al.* [1998] is due to the slower decrease of the oceanic pCO_2 in the model compared to the linear decrease hypothetized by *Bates et al.* [1998]. *Koch et al.* [2009] also estimated the $\tilde{\Delta}F_{CO_2}$ caused by Felix during the two-days of the storm with a regional model, forced with daily NCEP winds. They found a lower value than *Bates et al.* [1998] of 32 mmoleC m^{-2}, which they attribute to the underestimation of their model wind forcing. In a second step, to account for the post-storm effect, we integrate the impact of TC Felix over two weeks. In this case, the increase of the

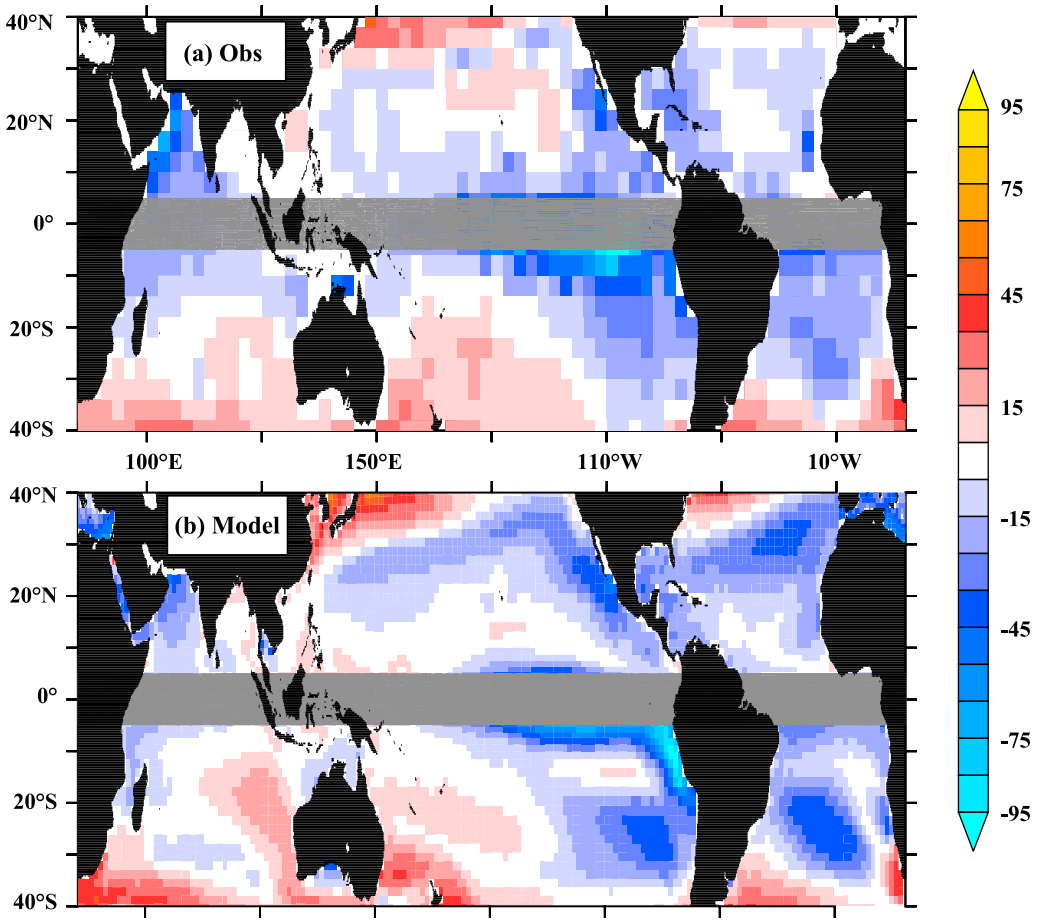

Figure 3. Evaluation of $DpCO_2$ during cyclonic season. $DpCO_2$ climatology (in μatm) during the cyclonic season (MJJASO in the northern hemisphere and NDJFMA in the southern hemisphere) from (a) Observed estimates [*Takahashi et al.*, 2009] and (b) the model (C run) over the 1993–2007 period. The grey band is to mark the time discontinuity between the two hemispheres.

$\tilde{\Delta}F_{CO_2}$ during the TC passage is counter-balanced by an the increased during post-TC conditions by approximately half, which leads to the final estimate of 30 mmoleC m^{-2}. This post-storm effect was not accounted for in the estimates of *Bates et al.* [1998] and *Koch et al.* [2009].

[26] A situation similar to that observed at BATS by *Bates et al.* [1998] was reported by *Nemoto et al.* [2009] in the coastal East China Sea, from continuous temperature and pCO_2 measurements at a moored buoy. Because their buoy was located in a coastal area, we cannot directly compare their observations with our 2° model results. However, *Nemoto et al.* [2009] examined how the variations in wind and in pCO_2 affected the F_{CO_2}. They found, in agreement with our analysis at BATS, that the F_{CO_2} efflux is increased during the passage of the storm, because of the increase in wind speed, and is decreased after the storm has passed, because of the decrease of pCO_2. Nevertheless, their estimate of the impact of TCs on the F_{CO_2}, approximately 30 mmoleC m^{-2} per typhoon, only accounts for the wind effect.

4.2. Sign of $DpCO_2$ Under TCs

[27] The efflux observed at BATS during TC Felix results from the negative $DpCO_2$ at the time t_0 of the TC passage. Previous studies that attempted to estimate the global impact of TC on F_{CO_2} have generalized this observation, hypothesizing that $DpCO_2$ at t_0 was negative for all TCs. Our numerical experiment allows to check this hypothesis (Figure 5): we found almost as many occurrences of negative and positive $DpCO_2$ at t_0 (25773 versus 21178 cases). The immediate consequence is that TCs do not systematically cause CO_2 effluxes at t_0 (as in BATS) but are also be responsible for influxes, in similar proportion (Figure 5b). Moreover, $|DpCO_2|$ at t_0 is larger than 10 μatm in ~50% of the cases, and cause the largest F_{CO_2} anomalies (tails of the distribution in Figure 5b). In the other ~50% cases, the impact of TC on the F_{CO_2} is small because $DpCO_2$ is close to zero.

[28] The spatial distribution of the positive and negative $DpCO_2$ cases under TCs in the C-run is displayed in Figures 6a and 6b. Areas with negative $DpCO_2$ during the cyclonic seasons are found mostly in the Western North Atlantic, Western and Eastern North Pacific, Arabian Sea and South West Indian Ocean, while areas of positive $DpCO_2$ are mostly in the Westernmost North Pacific, central south Indian Ocean, Bay of Bengal and South western Pacific, in broad agreement with the pCO_2 distribution during the cyclonic season (Figure 3). The same diagnostic applied to the climatology of *Takahashi et al.* [2009]

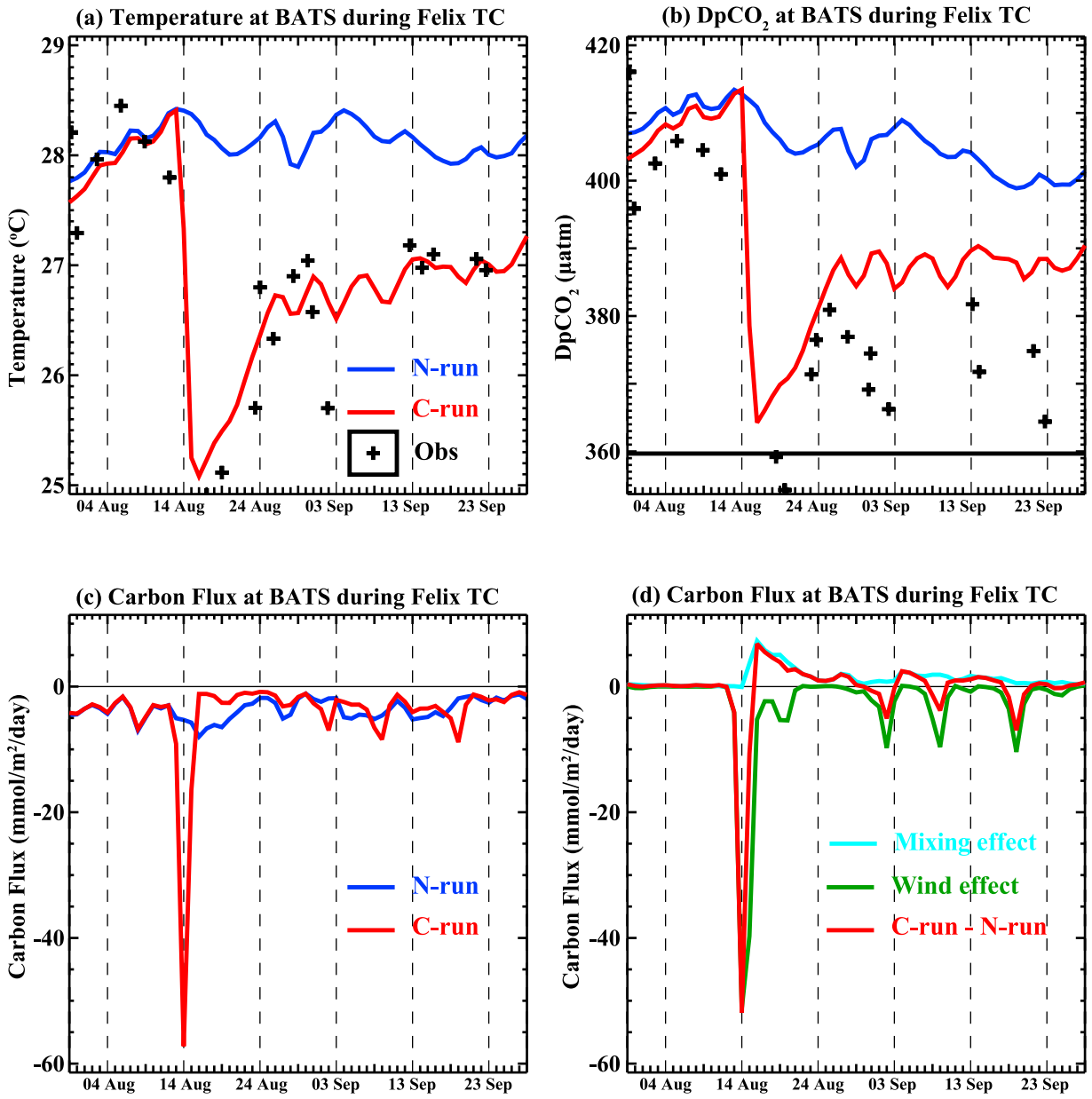

Figure 4. Hurricane Felix test case (BATS, August 1995). Temporal evolution of (a) SST and (b) oceanic pCO2 (in μatm) in the C run (red), the N run (blue) and shipboard measurements from *Bates et al.* [1998] (dots) during the passage of Hurricane Felix in the Sargasso Sea near Bermuda in August 1995. (c) Temporal evolution of the air-sea CO_2 flux (negative when oriented from the ocean to the atmosphere in mmole/m^2/day) for the C run (red) and the N run (blue) (d) Temporal evolution of the flux difference between the C and N runs (red), flux anomaly related to the TC wind effect (green), flux anomaly related to the TC mixing effect (blue) (computed according to section 2.4).

interpolated in time reveals similar regional patterns (Figures 6c and 6d). The differences are due both to model imperfections and to the absence of interannual variations in the climatology.

4.3. TCs Induced $DpCO_2$ and F_{CO_2} Anomalies

[29] Since the F_{CO_2} response differ depending on the sign of the $DpCO_2$ background conditions at the time of TCs passage, two different cases are considered in the following: the case where $DpCO_2$ is negative at t_0, causing an efflux to the atmosphere (case of BATS), and the opposite case, where $DpCO_2$ is positive at t_0, causing an influx to the ocean. Figure 7 shows the composite evolution of wind speed, SST, $DpCO_2$ and F_{CO_2} anomalies associated with the passage of all TCs falling in each category, and computed following section 2.4.

[30] In the two cases, the composite time-evolution of the wind, SST and $DpCO_2$ TC-induced anomalies are consistent

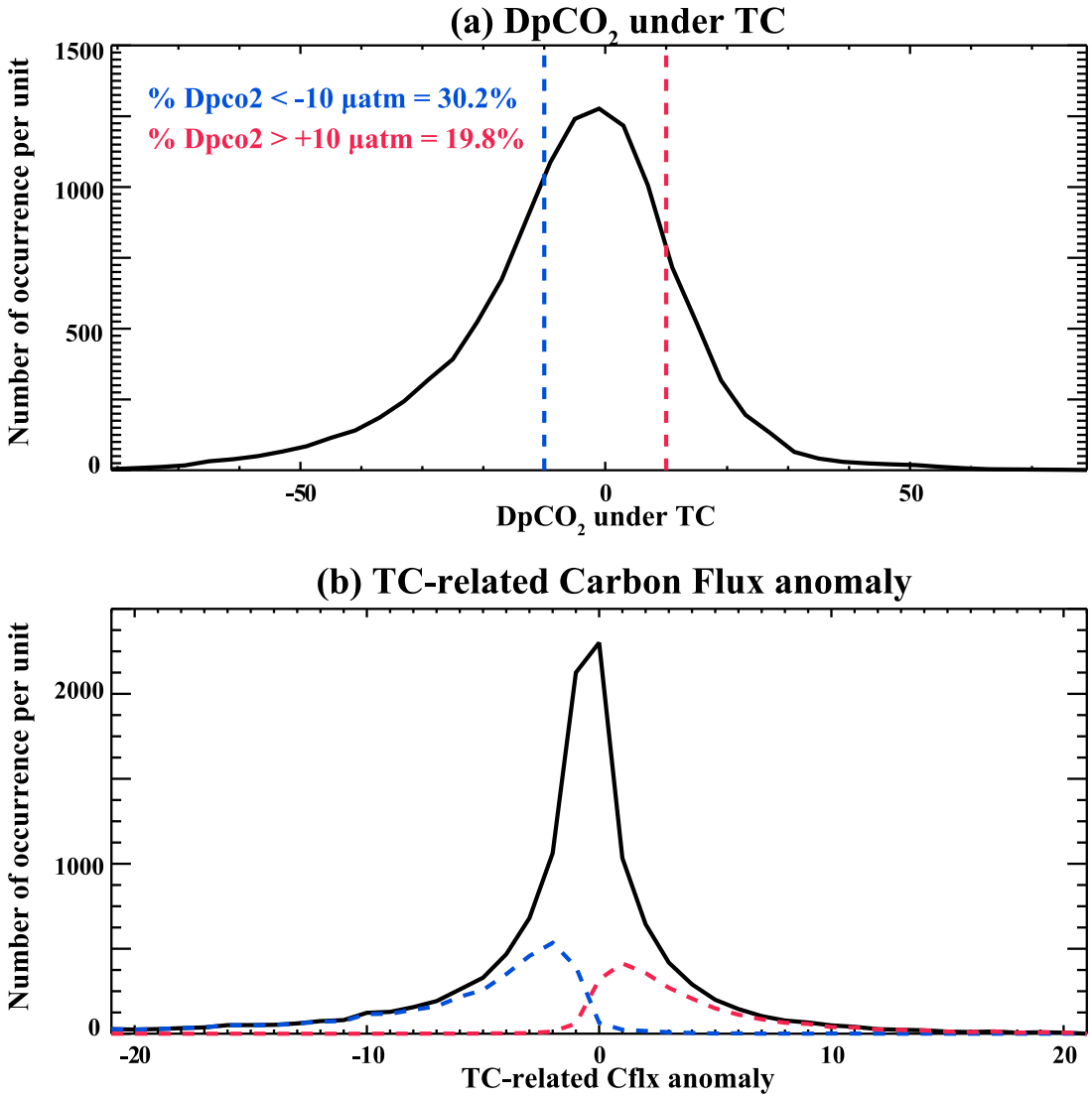

Figure 5. Distribution of $DpCO_2$ under TCs. Histograms of (a) $DpCO_2$ (in μatm) and (b) TC-related air-sea flux anomaly (in mmole/m^2/day) under TCs at time of maximum wind intensity for 46951 TC locations along 1663 TC tracks over the 1993–2007 period. Blue (red) curve on Figure 5b correspond to the histogram of TC-related air-sea flux anomaly under cyclones where $DpCO_2 < 10$ μatm ($DpCO_2 > 10$ μatm) corresponding to 30.2% (19,8%) of the cases.

with the results obtained in the case of TC Felix at BATS: TCs induce a cooling of the SST (Figure 7b), which reaches its maximum amplitude two to three days after the maximum wind speed intensity and slowly returns to its pre-storm value during the month that follows the passage of the TC. In our simulation, the maximum coolings reach 4°C, and the mean cooling when averaged over all TCs is less than 1°C. In agreement with [*Vincent et al.*, 2012], this cooling mainly results from the entrainment of cold sub-surface waters driven by the storm, especially for the strongest wind forcing. The mean cooling is larger in the negative $DpCO_2$ case, because the most intense TCs (and most intense coolings) occur over the NE Pacific (between 20–30°N) and NW Pacific (between 20–30°N), where the $DpCO_2$ is negative. Vertical mixing not only decreases SST but also, in agreement with the theoretical pCO_2 change with temperature [*Sarmiento and Gruber*, 2006], decreases pCO_2 and thus increases $DpCO_2$ (Figure 7c). The DpCO2 anomaly thus has the same sign in the undersaturated and supersaturated case (Figure 7c). Note that, rather counter intuitively, in the undersaturated case, the post-storm pCO2 decreases despite an influx of CO2 during and after the storm. This is because the temperature effect largely prevails over the increase of total inorganic carbon associated to the air-sea flux. Moreover, as for SST, the maximum magnitude of the pCO_2 drawdown is reached 2 to 3 days after the passage of the storm (Figure 7c), and the change is larger in the negative $DpCO_2$ case.

[31] Because the pre-storm air-sea fluxes have different signs in the two cases, the direct impact of TC winds on the air-sea CO_2 fluxes are opposite. At t_0, TC winds acts to increase the amplitude of the flux in either direction, thus

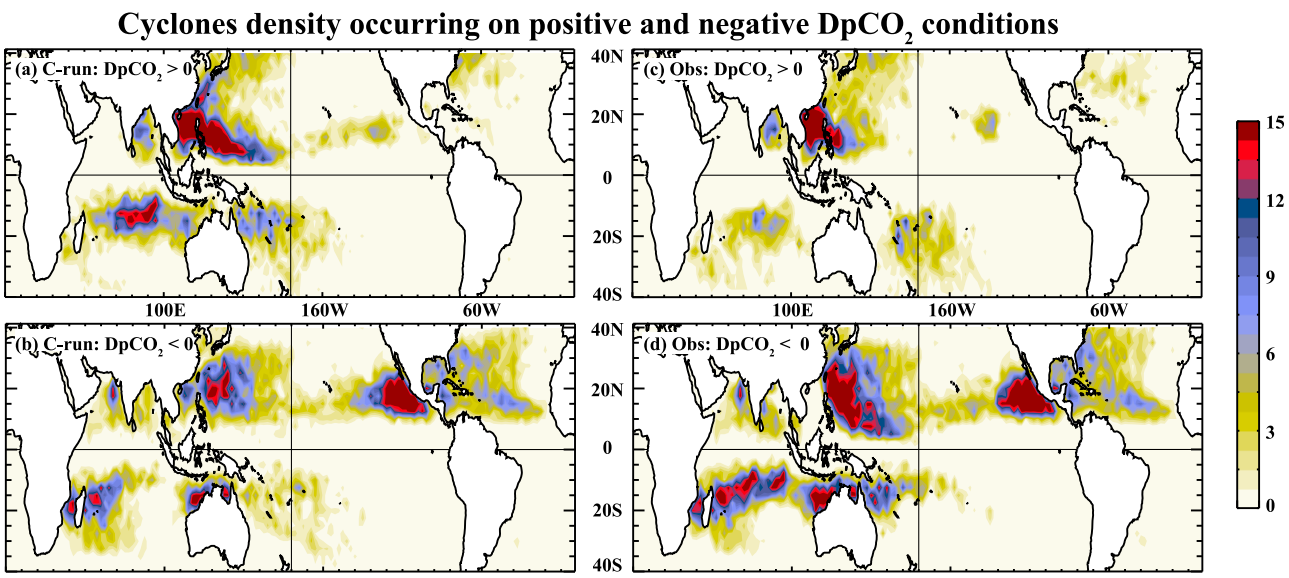

Figure 6. Locations where $DpCO_2$ is positive and negative under TCs. Density distribution (in cyclone-day/year) for TCs where (a) $DpCO_2 > 0$ and (b) $DpCO_2 < 0$ at $t = t_0$, t_0 being the time of maximum wind intensity. Densities are computed over the 1993–2007 period. (c and d) Same diagnostics applied to the $DpCO_2$ climatology of *Takahashi et al.* [2009] interpolated in time.

enhancing effluxes in the case of negative $DpCO_2$, and enhancing influxes in the case of positive $DpCO_2$ (Figure 7). After the storm, the decrease of pCO_2 causes $|DpCO_2|$ to decrease in the negative $DpCO_2$ (undersaturated) case (and eventually change sign), and to increase in the positive $DpCO_2$ (oversaturated) case (Figure 8); consequently, the amplitude of the flux is reduced in the oversaturated case (and eventually reverses), and is increased in the undersaturated case, in comparison with pre-storm conditions (Figures 7 and 8).

4.4. Respective Influence of TCs Wind and Induced Mixing on F_{CO_2}

[32] To assess and quantify the impact of TCs on F_{CO_2}, the wind and mixing effects have been separated according to equations (2), (3), and (4) for each TC, and averaged out for all oversaturated (resp. undersaturated) cases (Figure 9). In both cases, the wind effect explains most of the increase of the flux in either direction during the TC-passage, while the mixing effect explains the modifications of the flux after the storm, in opposite sign in the case of oversaturation, and in same sign in the case of undersaturation.

[33] In the oversaturated case, when integrated over 30 days, the time integral of the TC-induced flux anomaly is 1.1 mmole/m^2 and is positive. This means that, on average over all TCs, the negative wind-driven flux anomaly during the storm is more than offset by the post-storm, positive, mixing-driven flux anomaly. In the undersaturated case, the time integral of the TC-induced flux anomaly is 10.1 mmole/m^2; in this case, the wind-driven and mixing-driven anomalies are both positive and add up.

4.5. Regional and Global Impact of TC on F_{CO_2}

[34] In Figure 10, the storm and post-storm impacts of TCs on F_{CO_2} are evaluated regionally. This is done by integrating ΔF_{CO_2} over two time periods.

[35] During the storm peak intensity (t_0 − 1.5d to t_0 + 1.5d, Figure 10b), the averaged TC-driven flux anomaly is negative in the North West Atlantic, North West Pacific, North East Pacific, Arabian Sea and South West Indian, and is positive in the Westernmost North Pacific, central south Indian Ocean, Bay of Bengal and South western Pacific. These patterns are due to the first (resp. second) regions being predominantly supersaturated (resp. undersaturated) during the cyclonic season (Figure 3). After the storm (t_0 + 1.5d to t_0 + 30d, Figure 10c), the flux anomaly is systematically positive (except for a small region in the north eastern Pacific, where pCO_2 is enhanced by vertical mixing) and its pattern is that of the TC density. When considering the whole period (t_0 − 1.5d to t_0 + 30d, Figure 10a), the storm and post-storm effects often balance when they are of opposite signs.

[36] In consequence, in the North West Atlantic and Arabian Sea, which are mostly supersaturated during the cyclonic season, the net effect of TC on F_{CO_2} during the cyclonic season is very weak because the storm and post-storm effects almost compensate. The situation is different in the North West Pacific, where the strongest SST anomalies occur (Figure 2); because of these strong SST anomalies, the post-storm effect prevails over the storm effect, with the consequence of a net TC-induced CO_2 influx anomaly. In regions which are predominantly undersaturated during the cyclonic season, the storm and post-storm effects reinforce each other. Consequently, the mean effect of TC in the Westernmost North Pacific, central south Indian Ocean, Bay of Bengal and South western Pacific is to increase the uptake of CO_2 by the ocean during the cyclonic season.

[37] Tables 1 and 2 provide more quantitative numbers of the impact of TCs on F_{CO_2} over the large regions delimited in Figure 10a. Except in the North West Pacific and in the Bay of Bengal, the flux due to TC is generally less than

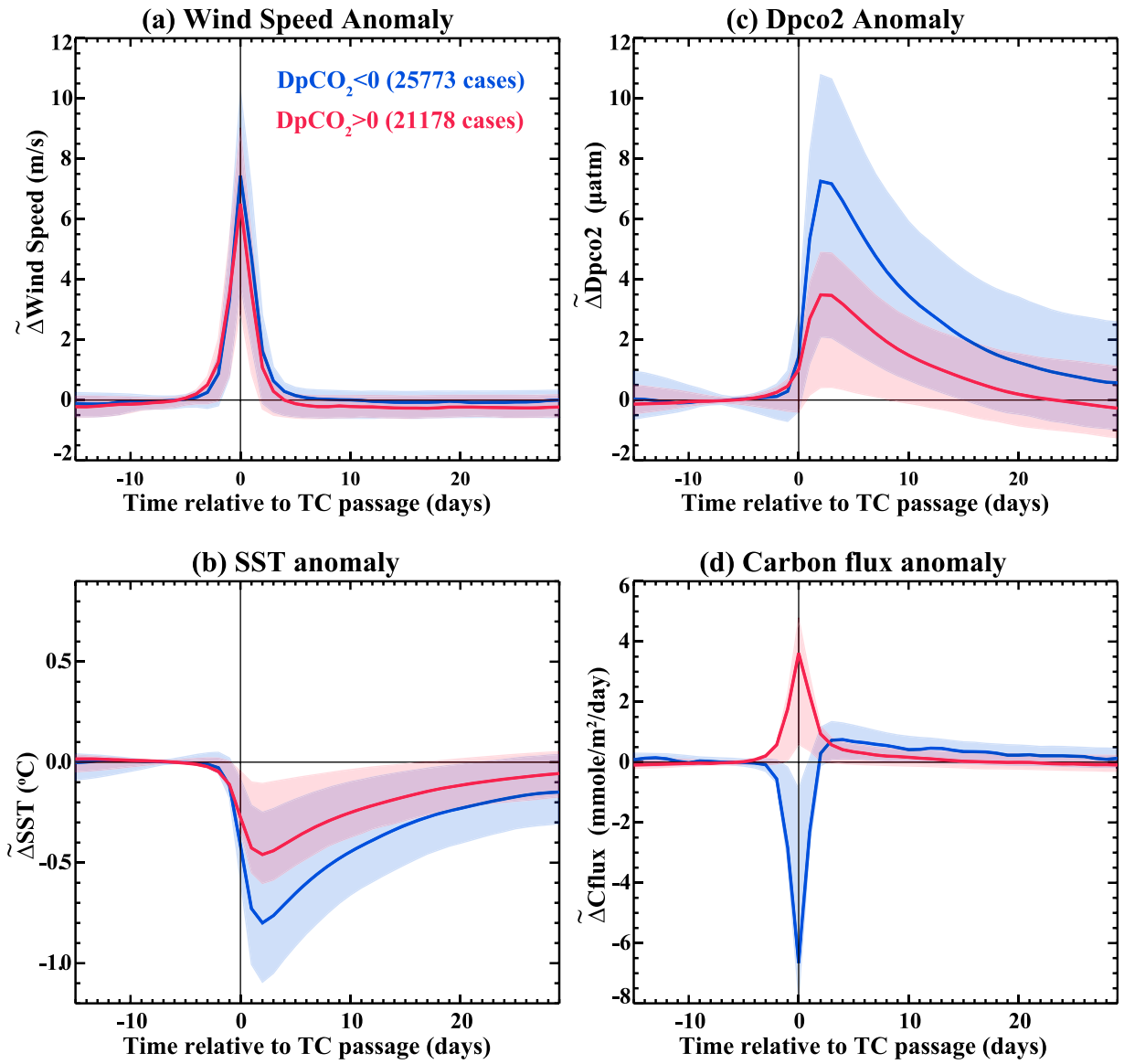

Figure 7. Composite time evolution of wind speed, SST, $DpCO_2$ and air-sea flux anomalies generated by the passage of TCs. Blue color: Mean composite of all cases (25773) where $DpCO_2 < 0$ at $t = t_0$, with t_0 the time of maximum wind intensity. Red color: Mean composite of all cases (21,178) where $DpCO_2 > 0$ at $t = t_0$. Shading show the $\pm 1/2$ standard deviation around the mean composite value. Composites are computed over the 1993–2007 period. Anomalies are computed according to section 2.4.

±3% of the total flux. In the North West Pacific and Bay of Bengal the percentage is larger (+33.4% and −13.6%, respectively) but they concern regions which weakly (15.5 and −0.6 TgC, respectively) contribute to the total F_{CO_2} during the cyclonic season (−305 TgC). Note also that in most regions, the flux due to TCs is not systematically in the same direction (Table 2); for instance, the North Atlantic is submitted to an average of 80 TC-days over supersaturated conditions, contributing to a TC efflux of −1.6 TgC, but also to 16 TC-days over undersaturated regions, which cause an influx of +1 TgC. Under undersaturated conditions, the TC induced flux is always positive, while it can be either positive or negative under supersaturated conditions (depending on the relative strength of the storm and post-storm effects) (Table 2). The North West Pacific and Bay of Bengal are predominantly undersaturated, which explains the larger % of the TC-flux to the total flux.

5. Discussion

5.1. Comparison With Previous Estimates

[38] The global impact of TCs on air-sea CO_2 fluxes estimated in this study (0.007 $Pg\ C\ y^{-1}$, i.e. 2% of the mean, subtropical flux during the cyclonic season, Table 1) is one order of magnitude less than the lowest previous estimates [*Perrie*, 2004; *Bates*, 2007; *Koch et al.*, 2009; *Huang and Imberger*, 2010] and is in opposite direction (influx anomaly). This is because previous estimates did not account for

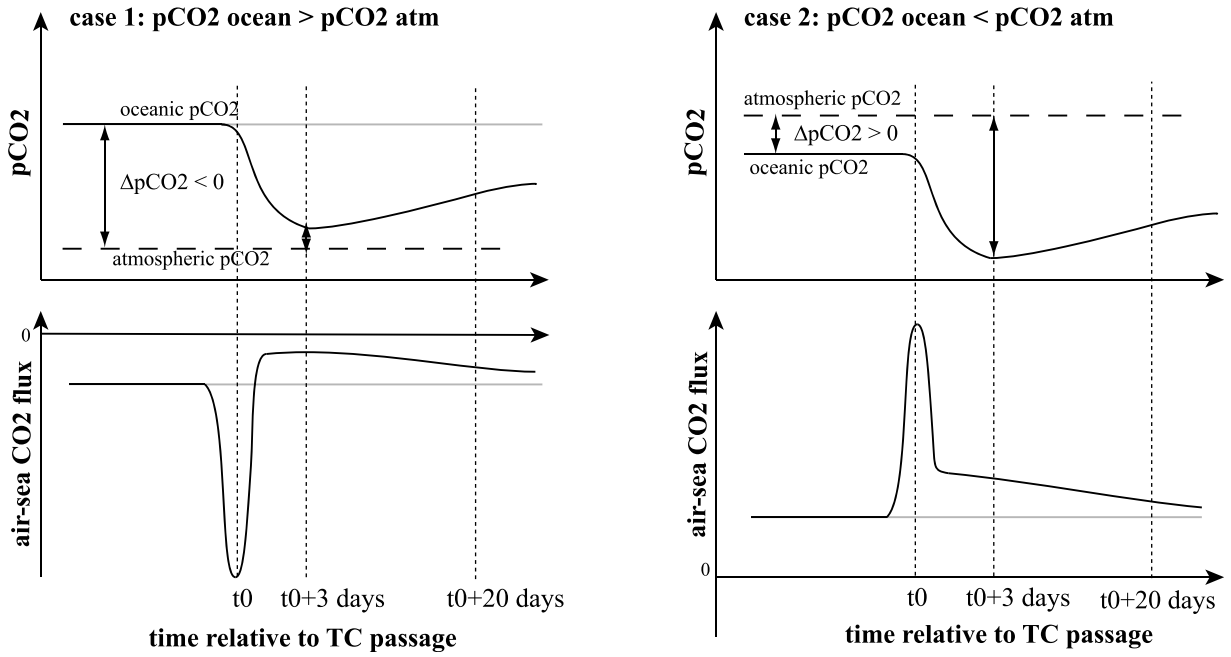

Figure 8. Schematic representation of the impact of TCs on pCO_2 and air sea flux. Schematic time evolution of oceanic pCO_2 and air-sea CO_2 flux associated with the passage of a TC (black curves). For reference, the grey curves show the stationary situation in the absence of TC. Day t_0 is the time of maximum wind intensity during the passage of TC. The left column is the case where the oceanic pCO_2 is initially larger than the atmospheric pCO_2 and the air-sea flux is directed from the ocean to the atmosphere (case of BATS). The right column is when the atmospheric pCO_2 is initially larger than the oceanic pCO_2 and the air-sea flux is directed from the atmosphere to the ocean.

two important aspects: first, in supersaturated regions, they did not account for the post-storm mixing-effect, which balances the storm wind-effect; second, they did not consider the impact of TCs over undersaturated regions.

[39] Previous estimates of air-sea CO_2 fluxes under TCs mainly focused on hurricanes in the North West Atlantic [*Bates et al.*, 1998; *Perrie*, 2004; *Bates*, 2007; *Koch et al.*, 2009; *Huang and Imberger*, 2010], with the exception of one study in the East China Sea [*Nemoto et al.*, 2009]. These

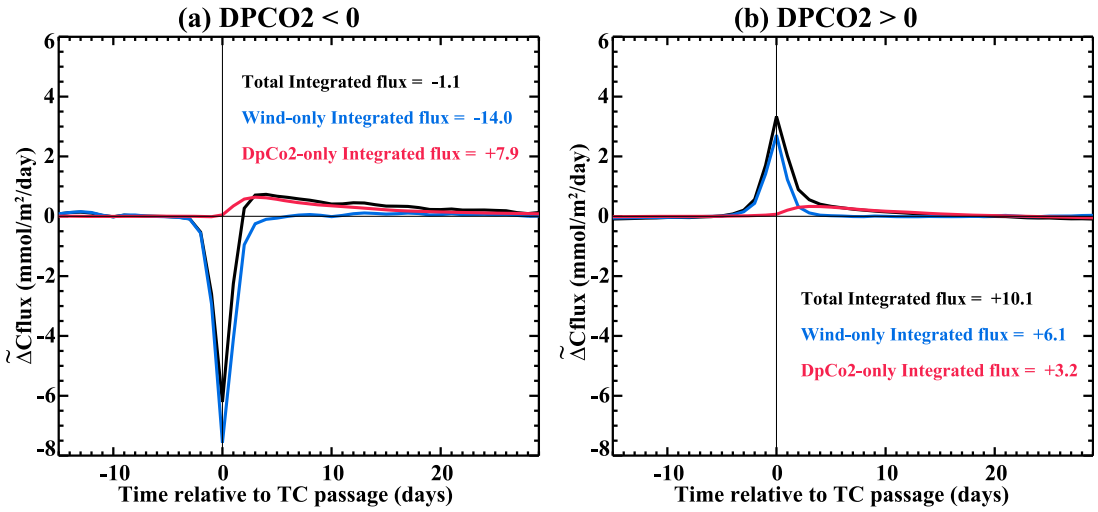

Figure 9. Composite time evolution of TC-induced air-sea flux anomalies: controlling mechanisms. Mean of all cases where (a) $DpCO_2 < 0$ at $t = t_0$ and (b) $DpCO_2 > 0$ at $t = t_0$, t_0 being the time of maximum wind intensity. Anomalies are computed over the 1993–2007 period. The black curve is the total TC-induced flux anomaly, the blue curve is the wind effect on the flux (section 2.4, equation (2)), the red curve is the mixing effect on the flux (section 2.4, equation (3)).

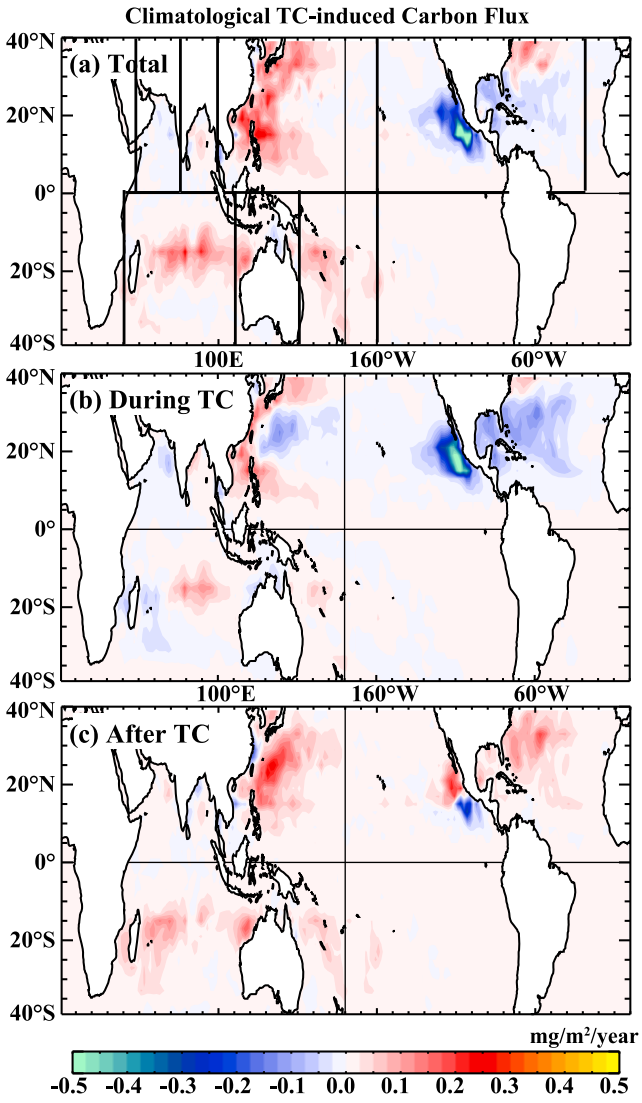

Figure 10. Climatological TC-induced air-sea flux. Climatological average of seasonally cumulated air-sea flux (in mmol/m^2/season) induced by cyclones along their tracks in the C-run between (a) $t_0 - 1.5d$ and $t_0 + 30d$ (b) $t_0 - 1.5d$ and $t_0 + 1.5d$ (c) $t_0 + 1.5d$ and $t_0 + 30d$. Dashed lines on Figure 10a indicate the boundaries of the regions discussed in Tables 1 and 2.

studies took place in undersaturated regions. In most of them, it was attempted to extrapolate the results from a few TCs (one to three TCs, typically) to the global ocean, by using TCs database and making assumptions about storm area, wind speed and oceanic pCO_2 values. Moreover, it was generally assumed that the oceanic conditions at the time and location of TC passage did not significantly deviate from the case study that was examined. The different assumptions and methods used led to a wide range of estimates. The first annual, global estimate by *Bates et al.* [1998] was a TC-induced efflux of up to 0.51 Pg C. Later, *Bates* [2007] estimated a smaller efflux of 0.04–0.08 Pg C, but no details on the method were provided. The method of *Huang and Imberger* [2010], with different extrapolation assumptions, lead to an efflux of 0.047–0.141 Pg C. *Nemoto et al.* [2009] restricted their extrapolation to the western

Table 1. Regional and Global CO_2 Fluxes and Contribution of TCs[a]

	Total Flux	TC-Flux	% TC/Total	STD (Total/TC)
North Atlantic	−65.7 (−2699)	−0.6	+1%	11.1/1.8
North East Pacific	−130.0 (−4988)	−3.0	+2.3%	24.3/2.9
North West Pacific	+15.5 (+384)	+5.2	+33.4 %	21.8/2.3
Bay of Bengal	−0.6 (−117)	+0.1	−13.6 %	4.3/0.3
Arabian Sea	−43.4 (−2727)	−0.1	+0.2 %	6.1/0.2
South Indian	+93.1 (+2838)	+2.7	+2.9 %	26.8/1.2
Australia	+ 18.1 (+2017)	+0.5	+2.5 %	5.0/0.4
South Pacific	+53.3 (+2492)	+1.7	+3.2%	18.2/ 1.0
Total	−305.0 (−1258)	+6.7	−2.2%	85.0/5.0

[a]Mean and standard deviation of total and TC-induced carbon flux cumulated over the cyclonic season and over different oceanic basins (delimited in Figure 10a), in Tera gC/cyclonic season. The STD represents interannual variations. The Total flux is computed over the region 40S-40N for the cyclonic season (NDJFMA for Southern Hemisphere and MJJASO for Northern Hemisphere). Value in parenthesis in the first column are in mgC/m^2.

subtropical North Pacific, and found a contribution of TCs equal to 76% of the summer efflux, a value even larger than the 20–54% estimate of *Bates et al.* [1998]. Our estimate in for North West Atlantic is close to zero (1%, Table 1), because the wind and mixing effect are in balance. In the North West Pacific, we found a larger impact (−37%, Table 1) but with opposite sign, because the mixing effect is larger than the wind effect. In that respect, our results are thus significantly different from the previous estimates.

[40] Moreover, it was hypothetized that the year-to year differences in TC frequency and intensity might be an important mechanism for controlling interannual variability in F_{CO_2} [*Bates et al.*, 1998; *Bates*, 2007], although this hypothesis was not supported by the model result of *Koch et al.* [2009] in the subtropical North Atlantic. To examine this question over different ocean sub-basins, we compared the standard deviation of the year-to-year regional F_{CO_2} budget to the standard deviation of the year-to-year regional TC-induced F_{CO_2} flux (Table 1). Our result extend the conclusion of *Koch et al.* [2009]: over the different sub-basins, TC explain between 0 and 10% of the interannual flux changes, with a global mean of ∼5 %.

Table 2. Global and Regional CO_2 Fluxes due TCs Depending on Oceanic State[a]

	TC-Flux $\Delta pCO_2 > 0$	TC-Flux $\Delta pCO_2 < 0$	Days $\Delta pCO_2 > 0$	Days $\Delta pCO_2 < 0$
North Atlantic	+1.0	−1.6	16	80
North East Pacific	+0.3	−3.3	14	93
North West Pacific	+5.2	0.0	168	119
Bay of Bengal	+0.1	0.0	15	8
Arabian Sea	0.0	−0.1	0	13
South Indian	+2.5	+0.2	77	66
Australia	+0.5	0	19	27
South Pacific	+1.5	+0.2	45	24
Total	11.3	−4.6	354	430

[a]Mean TC-induced carbon flux cumulated over the cyclonic season (NDJFMA for Southern Hemisphere and MJJASO for Northern Hemisphere) and over different oceanic basins (delimited in Figure 10a). For each region, we count the number of TCs occurrences (In days/cyclonic season) and associated carbon flux (in Tera gC/cyclonic season) over undersaturated (versus oversaturated) oceanic state.

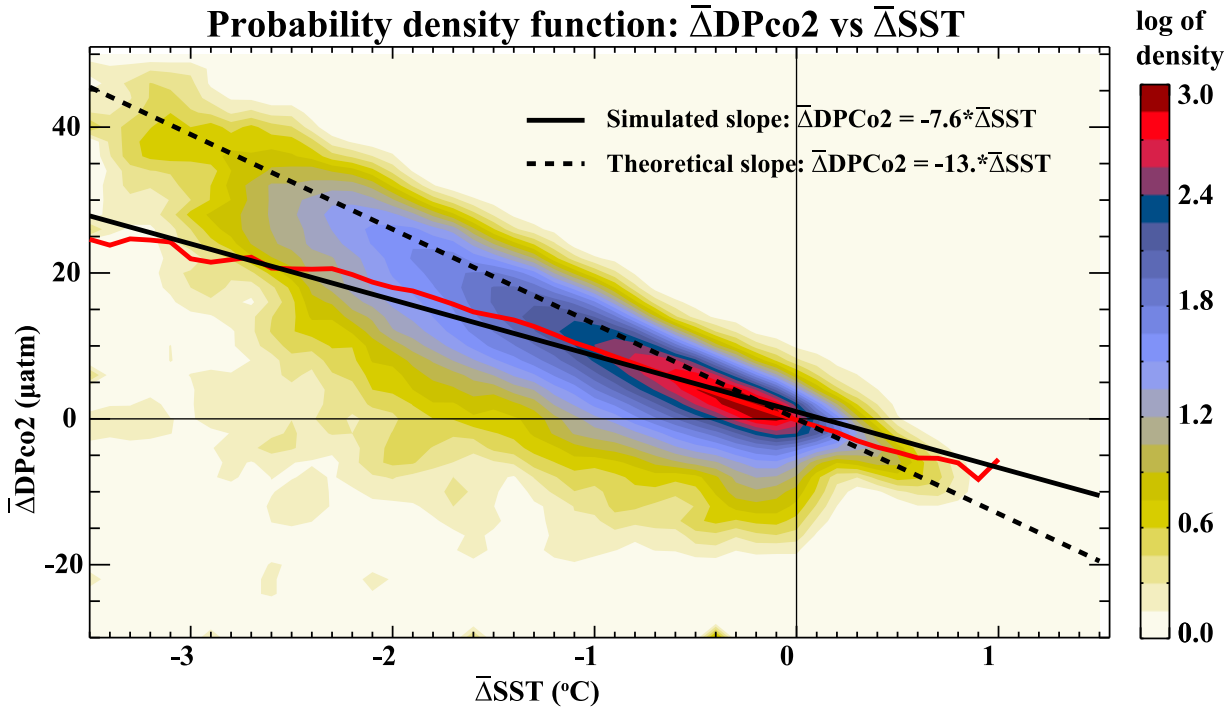

Figure 11. TC-induced $DpCO_2$ anomaly versus SST anomaly. Probability Density function of TC-induced $DpCO_2$ wake anomaly versus SST wake anomaly simulated in the model. Thick black line indicates the theoretical relationship of Gruber and Sarmiento, with a slope of −13. The blue line is the mean $\overline{\Delta}$SST per bin of $\overline{\Delta}DpCO_2$. The black line is the linear fit to the blue line and as a slope of −7.6. Anomalies are computed over the 1993–2007 period along TC tracks for run C.

5.2. The Post-Storm, Mixing Effect

[41] One of the important process highlighted in this study is the impact of TC-induced vertical mixing with thermocline waters, which occurs essentially after the storm, cools the SST and reduces the pCO_2. The importance of this processes is revealed by the persistence of the cold SST anomaly after the passage of the storm that can last from a few days to over a month. This persistence is accurately reproduced by our model when compared with satellite AMSR observations. The link between the cooling and the change in pCO_2 is however not straightforward. Figure 11 shows the distribution of the change in pCO2 after the passage of TC, against the change in SST (computed following section 2.4 as $\overline{\Delta}pCO_2$ versus $\overline{\Delta}T$). It confirms that in most cases, pCO_2 decreases after the passage of TCs; the average decrease (−7.6 μatm per °C) is however smaller than the theoretical decrease due to the temperature effect alone (−13 μatm per °C, *Sarmiento and Gruber* [2006]). This feature can be explained by the entrainment of higher DIC water from the thermocline into the surface mixed-layer which increases the pCO_2 and partly offsets the temperature effect; TC can also alleviate nutrient limitation and promote phytoplankton blooms [*Babin et al.*, 2004; *Walker et al.*, 2005; *Son et al.*, 2006; *Patra et al.*, 2007; *Liu et al.*, 2009; *Hanshaw et al.*, 2008; *Gierach and Subrahmanyam*, 2008], thus decreasing the pCO2. How mixing of these different elements impact pCO_2 depends on their respective vertical gradients and is spatially and temporally variable [*Mahadevan et al.*, 2011]. Our model results are in that respect consistent with the analysis of *Mahadevan et al.* [2011], based on climatological distributions of T, S, DIC, nutrients and TA, which suggest that the temperature impact on pCO_2 prevails upon the change of the other variables (S, TA, DIC) in the tropical oceans and during the summer cyclonic season. However, a sharp rise in pCO_2 has recently been reported after the passage of typhoon Choi-Wan in 2009 in the North West Pacific, which preceded the drop in temperature by about 6 h [*Bond et al.*, 2011]. Such short-term sequence could not be examined with the daily resolution of our model outputs and deserves further investigation.

5.3. Caveats

[42] Our results rely on an number of assumptions that were made to build the model. An inherent limitation of our modeling strategy is that the analytical formulation of TC winds derived from *Willoughby et al.* [2006] does not account for the vast variety of wind structures associated with TCs. The latest version of the IBTrACS database provides radius estimations for some TCs, which could be a first step in better defining the geometry of the wind. The wind forcing asymmetry due to the translation speed of TCs has also not been accounted for in our modeling strategy: including this effect may also improve characteristics of the simulated TC-induced cooling, in particular for fast cyclones. Another factor that was not accounted for is the intense rain falls that often come with TCs, and can dilute the salinity and DIC, with possible modifications of the surface pCO_2. A more precise estimate of the TC induced F_{CO_2} would certainly require to examine this aspect.

[43] Regarding model resolution, as shown by *Vincent et al.* [2012], a 2° resolution reasonably captures the transfer of cyclone kinetic energy to the upper ocean (their Figure 2), which is the main driver of mixing, a dominant process in the cold wake formation. However, their analysis also suggests that the maximum amplitude of Ekman pumping near the eye, a process which is also involved in the cold wake formation but is less dominant [*Greatbatch*, 1985; *Yablonsky and Ginis*, 2009; *Jullien et al.*, 2012], is strongly underestimated with a resolution of 2°. Moreover, a resolution of 2° is not sufficient to explicitly resolve oceanic mesoscale eddies, which, as discussed in previous studies [e.g., *Shay et al.*, 1992; *Jaimes et al.*, 2011], can modulate the SST response to TCs. Although we have shown that our 2° resolution model reasonably captures the magnitude of the TC-induced cooling, a main factor affecting the FCO_2, further studies at higher resolution would be needed to strengthen our results and evaluate the role of the small scale oceanic processes that were not accounted for in the present study.

[44] Decreasing atmospheric pCO_2 during the passage of TCs, associated with the decrease atmospheric pressure, have been reported [*Bates et al.*, 1998; *Huang and Imberger*, 2010], with values up to 20 μatm (V.V.S.S. Sarma, unpublished data, 2011). In our model, the atmospheric pCO_2 is increased from year to year but is not impacted by TCs. The model study of *Huang and Imberger* [2010], which accounts for that effect, suggest that it is very short-lived (<12 h) and limited to the core of the TC (in a 50 km radius); we thus expect this effect to be weak when averaged over the large oceanic area influenced by TCs.

[45] Our results are also certainly dependent on the choice of the parameterization of the gas transfer velocity at hight wind speed, as suggested by the sensitivity analysis of *Perrie* [2004]. A different choice might imply larger absolute values of the fluxes, and modulate the strengths of the compensations.

6. Conclusion

[46] In this study, we used a state-of-the-art global ocean biogeochemical model driven by TC wind forcing derived from a historical TC database. This allows us to examine the ocean response along 1,663 TC tracks over the 1993–2007 period. The resulting modeled SST response to TCs compares very well with satellite estimates during the same period. The model also accurately reproduces the sharp pCO_2 drawdown recorded after the passage of Hurricane Felix in 1995 in the NW Atlantic.

[47] Previous case studies have illustrated the strong influence of TCs on ocean-atmosphere CO_2 fluxes by increasing the gas exchange coefficient and decreasing the SST and oceanic pCO_2. Moreover, it was generally assumed that the ocean is oversaturated in CO_2 under TCs, because TCs blow essentially in the tropics during the summer season. Thus, based on a these few observations, it has been suggested that TCs significantly increase the CO_2 efflux from the ocean to the atmosphere. However, limited availability of pCO_2 observations under TCs harsh conditions has so far restricted global quantification of the TC-induced F_{CO_2} to hazardous extrapolations.

[48] We found a similar proportion of TCs over undersaturated regions (∼20% of TC locations are over regions where $DpCO_2 < -10$ μatm) and oversaturated regions (∼30% for $DpCO_2 > 10$ μatm), with a large proportion (∼50%) of TCs over regions where the ocean and atmosphere are in near equilibrium. This estimation, based on our model outputs, is consistent with a similar estimation from observed climatological pCO_2 variations. The consequence is that TCs can generate instantaneous CO_2 fluxes directed from the ocean to the atmosphere (efflux) or vise-versa (influx), depending on the oceanic condition at the time of the TC passage; this instantaneous flux is very weak in ∼50% of the cases.

[49] Moreover, we identify two competing effects of TCs on F_{CO_2} that are not synchronous. During the storm and depending on the sign of the difference of pCO_2 between the ocean and atmosphere, TCs are responsible for large efflux or influx anomalies due to the strong winds. During several weeks after the storm, oceanic pCO_2 is reduced in response to vertical mixing, which systematically causes an influx anomaly. Generally, the storm wind-effect and post-storm mixing effect have the same order of magnitude. This implies that, contrary to previous estimates, TCs weakly impacts the CO_2 efflux because the two effects oppose with each other when they blow over supersaturated areas (typically in the North Atlantic, North-East Pacific, Arabian Sea). In contrast, TCs increase the CO_2 influx because the two effects add up under undersaturated conditions (e.g. in the Westernmost North Pacific, Bay of Bengal, South Indian and Pacific Ocean). In total, we find that TCs account for ∼2% of the F_{CO_2} during the cyclonic season over the tropical ocean (40°N-40°S). This is an order of magnitude less than the lowest previous estimates. Moreover, we find that regionally, TC account for 0 to 10% of the year-to-year variations of the F_{CO_2}.

[50] **Acknowledgments.** This study was supported by IRD, CNRS, INSU (LEFE project CYCLOCEAN AO2010-538863), CNES (project CPUMP) and through EU FP7 project CARBOCHANGE (Changes in carbon uptake and emissions by oceans in a changing climate) which received funding from the European Community's Seventh Framework Programme under grant agreement 264879. This is NIO contribution 5131. Model development was supported by the NEMO system team. The study was initiated during M. Lévy, M. M. Lengaigne, and E. M. Vincent's stay at the NIO.

References

Aumont, O., and L. Bopp (2006), Globalizing results from ocean in situ iron fertilization studies, *Global Biogeochem. Cycles*, *20*, GB2017, doi:10.1029/2005GB002591.

Babin, S., J. Carton, T. Dickey, and J. Wiggert (2004), Satellite evidence of hurricane-induced phytoplankton blooms in an oceanic desert, *J. Geophys. Res.*, *109*, C03043, doi:10.1029/2003JC001938.

Bates, N. R. (2007), Interannual variability of the oceanic CO_2 sink in the subtropical gyre of the North Atlantic Ocean over the last 2 decades, *J. Geophys. Res.*, *112*, C09013, doi:10.1029/2006JC003759.

Bates, N. R., A. Knap, and A. Michaels (1998), Contribution of hurricanes to local and global estimates of air-sea exchange of CO_2, *Nature*, *395*(6697), 58–61.

Bond, N., M. Cronin, C. Sabine, Y. Kawai, H. Ichikawa, P. Freitag, and K. Ronnholm (2011), Upper ocean response to typhoon Choi-Wan as measured by the Kuroshio Extension Observatory mooring, *J. Geophys. Res.*, *116*, C02031, doi:10.1029/2010JC006548.

Chiang, T.-L., C.-R. Wu, and L.-Y. Oey (2011), Typhoon Kai-Tak: An ocean's perfect storm, *J. Phys. Oceanogr.*, *41*(1), 221–233, doi:10.1175/2010JPO4518.1.

Cione, J., and E. Uhlhorn (2003), Sea surface temperature variability in hurricanes: Implications with respect to intensity change, *Monthly Weather Rev.*, *131*, 1783–1796.

Cravatte, S., G. Madec, T. Izumo, C. Menkes, and A. Bozec (2007), Progress in the 3-D circulation of the eastern equatorial Pacific in a climate ocean model, *Ocean Modell.*, *17*(1), 28–48, doi:10.1016/i.ocemod.2006.11.003.

D'Asaro, E. (2003), The ocean boundary layer below hurricane Dennis, *J. Phys. Oceanogr.*, *33*(3), 561–579.

D'Asaro, E., and C. McNeil (2007), Air-sea gas exchange at extreme wind speeds measured by autonomous oceanographic floats, *J. Mar. Syst.*, *66*(1–4), 92–109.

Dickey, W. J. B. T. D. (2008), Observations and analyses of the upper ocean responses to tropical storms and hurricanes in the vicinity of Bermuda, *J. Geophys. Res.*, *113*, C08009, doi:10.1029/2007JC004358.

Donelan, M. A. (2004), On the limiting aerodynamic roughness of the ocean in very strong winds, *Geophys. Res. Lett.*, *31*, L18306, doi:10.1029/2004GL019460.

Gent, P. R., and J. C. McWilliams (1990), Isopycnal mixing in ocean circulation models, *J. Phys. Oceanogr.*, *20*, 150–155.

Gierach, M. M., and B. Subrahmanyam (2008), Biophysical responses of the upper ocean to major Gulf of Mexico hurricanes in 2005, *J. Geophys. Res.*, *113*, C04029, doi:10.1029/2007JC004419.

Greatbatch, R. J. (1985), On the role played by upwelling of water in lowering sea surface temperatures during the passage of a storm, *J. Geophys. Res.*, *90*, 11,751–11,755, doi:10.1029/JC090iC06p11751.

Griffies, S. M., et al. (2009), Coordinated ocean-ice reference experiments (cores), *Ocean Modell.*, *26*(1), 1–46, doi:10.1016/j.ocemod.2008.08.007.

Hanshaw, M. N., M. S. Lozier, and J. B. Palter (2008), Integrated impact of tropical cyclones on sea surface chlorophyll in the North Atlantic, *Geophys. Res. Lett.*, *35*, L01601, doi:10.1029/2007GL031862.

Huang, P., and J. Imberger (2010), Variation of pCO_2 in ocean surface water in response to the passage of a hurricane, *J. Geophys. Res.*, *115*, C10024, doi:10.1029/2010JC006185.

Jaimes, B., L. K. Shay, and G. R. Halliwell (2011), The response of quasi-geostrphic oceanic vortices to tropical cyclone forcing, *J. Phys. Ocean.*, *41*, 1965–1985.

Jullien, S., C. E. Menkes, P. Marchesiello, N. C. Jourdain, M. Lengaigne, A. Koch-Larrouy, J. Lefevre, E. M. Vincent, and V. Faure (2012), Impact of tropical cyclones on the south pacific ocean heat budget, *J. Phys. Oceanogr.*, in press.

Koch, J., G. A. Mckinley, V. Bennington, and D. Ullman (2009), Do hurricanes cause significant interannual variability in the air-sea CO_2 flux of the subtropical North Atlantic?, *Geophys. Res. Lett.*, *36*, L07606, doi:10.1029/2009GL037553.

Large, W. G., and S. G. Yeager (2009), The global climatology of an interannually varying air-sea flux data set, *Clim. Dyn.*, *33*(2–3), 341–364, doi:10.1007/s00382-008-0441-3.

Liss, P. S., and L. Merlivat (1986), Air-sea gas exchange rates: Introduction and synthesis, in *The Role of Sea-Air Exchange in Geochemical Cycling*, *NATO/ASI Ser.*, vol. 185, edited by P. Buat-Ménard, pp. 113–127, D. Reidel, Dordrecht, Netherlands.

Liu, X., M. Wang, and W. Shi (2009), A study of a Hurricane Katrina–induced phytoplankton bloom using satellite observations and model simulations, *J. Geophys. Res.*, *114*, C03023, doi:10.1029/2008JC004934.

Lloyd, I. D., and G. A. Vecchi (2011), Observational evidence for oceanic controls on hurricane intensity, *J. Clim.*, *24*(4), 1138–1153, doi:10.1175/2010JCLI3763.1.

Madec, G. (2008), Nemo ocean engine, *Note du Pole de modelisation de l'Institut Pierre-Simon Laplace*, *27*, 1–217, doi:ISSN:1288-1619.

Mahadevan, A., A. Tagliabue, L. Bopp, A. Lenton, L. Memery, and M. Lévy (2011), Impact of episodic vertical fluxes on sea surface pCO_2, *Philos. Trans. R. Soc. A*, *369*(1943), 2009–2025, doi:10.1098/rsta.2010.0340.

McNeil, C., and E. D'Asaro (2007), Parameterization of air-sea gas fluxes at extreme wind speeds, *J. Mar. Syst.*, *66*(1–4), 110–121.

Nemoto, K., T. Midorikawa, A. Wada, K. Ogawa, S. Takatani, H. Kimoto, M. Ishii, and H. Inoue (2009), Continuous observations of atmospheric and oceanic CO_2 using a moored buoy in the East China Sea: Variations during the passage of typhoons, *Deep Sea Res., Part II*, *56*(8–10), 542–553.

Patra, P. K., M. D. Kumar, N. Mahowald, and V. V. S. S. Sarma (2007), Atmospheric deposition and surface stratification as controls of contrasting chlorophyll abundance in the North Indian Ocean, *J. Geophys. Res.*, *112*, C05029, doi:10.1029/2006JC003885.

Perrie, W. (2004), The role of midlatitude storms on air-sea exchange of CO_2, *Geophys. Res. Lett.*, *31*, L09306, doi:10.1029/2003GL019212.

Price, J. (1981), Upper ocean response to a hurricane, *J. Phys. Oceanogr.*, *11*, 153–175.

Price, J. F., J. Morzel, and P. P. Niiler (2008), Warming of SST in the cool wake of a moving hurricane, *J. Geophys. Res.*, *113*, C07010, doi:10.1029/2007JC004393.

Samson, G., H. Giordani, G. Caniaux, and F. Roux (2009), Numerical investigation of an oceanic resonant regime induced by hurricane winds, *Ocean Dyn.*, *59*, 565–586.

Sarmiento, J., and N. Gruber (2006), *Ocean Biogeochemical Dynamics*, 564 pp., Princeton Univ. Press, Princeton, N. J.

Shay, L. K., P. Black, A. Mariano, J. Hawkins, and R. Elsberry (1992), Upper ocean response to hurricane gilbert, *J. Geophys. Res.*, *97*(20), 227–248.

Son, S., T. Platt, H. Bouman, D. Lee, and S. Sathyendranath (2006), Satellite observation of chlorophyll and nutrients increase induced by Typhoon Megi in the Japan/East Sea, *Geophys. Res. Lett.*, *33*, L05607, doi:10.1029/2005GL025065.

Takahashi, T., J. Olafsson, J. G. Goddard, D. W. Chipman, and S. C. Sutherland (1993), Seasonal variation of CO2 and nutrients in the high-latitude surface oceans: A comparative study, *Global Biogeochem. Cycles*, *7*(4), 843–878, doi:10.1029/93GB02263.

Takahashi, T., et al. (2009), Climatological mean and decadal change in surface ocean pCO_2, and net sea-air CO_2 flux over the global oceans, *Deep Sea Res., Part II*, *56*(8–10), 554–577.

Vincent, E. M., M. Lengaigne, G. Madec, J. Vialard, G. Samson, N. C. Jourdain, C. E. Menkes, and S. Julien (2012), Processes setting the characteristics of sea surface cooling induced by tropical cyclones, *J. Geophys. Res.*, *117*, C02020, doi:10.1029/2011JC007396.

Walker, N., R. Leben, and S. Balasubramanian (2005), Hurricane-forced upwelling and chlorophyll a enhancement within cold-core cyclones in the Gulf of Mexico, *Geophys. Res. Lett.*, *32*, L18610, doi:10.1029/2005GL023716.

Wanninkhof, R. (1992), Relationship between wind speed and gas exchange over the ocean, *J. Geophys. Res.*, *97*(C5), 7373–7382.

Wentz, F. J., C. Gentemann, D. Smith, and D. Chelton (2000), Satellite measurements of sea surface temperature through clouds, *Science*, *288*, 847–850.

Willoughby, H., and M. Rahn (2004), Parametric representation of the primary hurricane vortex. part I: Observations and evaluation of the Holland (1980) model, *Monthly Weather Rev.*, *132*, 3033–3048.

Willoughby, H., R. Darling, and M. Rahn (2006), Parametric representation of the primary hurricane vortex. part II: A new family of sectionally continuous profiles, *Monthly Weather Rev.*, *134*(4), 1102–1120.

Yablonsky, R. M., and I. Ginis (2009), Limitation of one-dimensional ocean models for coupled hurricane-ocean model forecasts, *Monthly Weather Rev.*, *137*, 4410–4419.

L. Bopp, LSCE-IPSL, Orme des Merisiers, CEA Saclay, F-91191 Gif Sur Yvette, France.

C. Ethé, M. Lengaigne, M. Lévy, G. Madec, and E. Vincent, LOCEAN-IPSL, UPMC, BC 100, 4 pl. Jussieu, F-75252 Paris CEDEX 05, France. (marina@locean-ipsl.upmc.fr)

D. Kumar, NIO, Dona Paula, Goa 403004, India.

V. V. S. S. Sarma, NIO, Visakhapatnam 530017, India.